Corbi, F., Funiciello, F., Brizzi, S., Lallemand, S., Rosenau, M. (2017): Control of asperities size and spacing on seismic behavior of subduction megathrusts. - *Geophysical Research Letters*, *44*, 16, pp. 8227—8235.

DOI: http://doi.org/10.1002/2017GL074182

AGU PUBLICATIONS

Geophysical Research Letters

RESEARCH LETTER
10.1002/2017GL074182

Key Points:
- We use analog models simulating along-strike rupture behavior of megathrust earthquakes, including asperities synchronization
- The barrier-to-asperity length ratio negatively correlates with maximum magnitude and seismicity rate
- The barrier-to-asperity length ratio controls the process of asperities synchronization and in turn the maximum earthquake magnitude

Supporting Information:
- Supporting Information S1

Correspondence to:
F. Corbi,
fabio.corbi3@gmail.com

Citation:
Corbi, F., F. Funiciello, S. Brizzi, S. Lallemand, and M. Rosenau (2017), Control of asperities size and spacing on seismic behavior of subduction megathrusts, *Geophys. Res. Lett.*, *44*, 8227–8235, doi:10.1002/2017GL074182.

Received 16 MAY 2017
Accepted 31 JUL 2017
Accepted article online 2 AUG 2017
Published online 19 AUG 2017

Control of asperities size and spacing on seismic behavior of subduction megathrusts

Fabio Corbi[1], Francesca Funiciello[2], Silvia Brizzi[2], Serge Lallemand[1], and Matthias Rosenau[3]

[1]Géosciences Montpellier, CNRS, University of Montpellier, Montpellier, France, [2]Laboratory of Experimental Tectonics, Roma Tre University, Rome, Italy, [3]Helmholtz Centre Potsdam-GFZ German Research Centre for Geosciences, Potsdam, Germany

Abstract The majority of the largest subduction megathrust earthquakes share the common characteristic of rupturing more than one asperity along strike of the margin. Understanding the factors that control coseismic failure of multiple asperities, and thus maximum magnitude, is central for seismic hazard assessment. To investigate the role of asperities size and spacing on maximum magnitude, seismicity rate, and percentage of synchronized ruptures, we use analog models simulating along-strike rupture behavior of megathrust earthquakes. We found negative correlations between the barrier-to-asperity length ratio *Db/Da* and maximum magnitude and seismicity rate. *Db/Da* also controls the process of asperities synchronization along the megathrust. A permanent barrier behavior is observed for $Db/Da > 0.5$. Comparing our experimental results to the Nankai Trough historical seismicity, we propose that the distribution of megathrust frictional heterogeneities likely explains the diversity of earthquakes which occurred there.

1. Introduction

The world's largest earthquakes occur on the shallow part of the subduction megathrust: the frictional interface between the subducting oceanic and overriding plates. Slip along the megathrust might be seismic or aseismic, tuned by a combination of parameters among which the presence of geometrical irregularities or stress fluctuations due to past earthquakes play an important role [*Avouac*, 2015; *Scholz and Campos*, 2012; *Wang and Bilek*, 2014]. Areas hosting large seismic slip are called asperities [e.g., *Lay and Kanamori*, 1981; *Lay et al*., 1982], and areas where the rupture propagation is inhibited are known as barriers. In the framework of rate-state friction [e.g., *Scholz*, 1998], asperities are characterized by velocity-weakening frictional behavior (i.e., the friction rate parameter $a\text{-}b < 0$) indicating that seismic rupture may nucleate and easily propagate, while barriers are characterized by velocity-strengthening frictional behavior (i.e., $a\text{-}b > 0$) that inhibits the seismic rupture propagation [*Scholz*, 1998].

According to the "asperity model" [*Lay and Kanamori*, 1981; *Lay et al*., 1982], the magnitude of an earthquake depends on the possibility for asperities to fail simultaneously during a single event (Figure 1a). Simultaneous failure requires equivalent stresses on neighboring asperities and may be the result of a synchronization process which occurs over multiple seismic cycles [e.g., *Ruff*, 1996]. Candidates for asperities synchronization include the 1960 Chile earthquake ($M_w = 9.5$) and the 2004 Sumatra-Andaman earthquake ($M_w = 9.2$), where multiple (> 4) high slip patches have been imaged by the inversion of geological and geophysical data [*Moreno et al*., 2009; *Subarya et al*., 2006]. Geodetic methods are widely used to infer the pattern of locked areas during the interseismic stage. These studies show that the pattern of interseismic coupling on subduction megathrusts is generally heterogeneous [e.g., *Chlieh et al*., 2008; *Moreno et al*., 2010], and coupled areas are tentatively interpreted as asperities failing during earthquakes [e.g., *Moreno et al*., 2010, *Schurr et al*., 2014, *Tilmann et al*., 2016]. However, the physical conditions that lead to simultaneous rupture of neighboring highly stressed patches and consequent triggering of a megathrust earthquake remain debated.

The process of asperities interaction by means of static stress transfer has been investigated with relatively simple analytical models of coupled spring sliders, where the two sliders represent individual fault segments. Despite the simplicity of such models, fault segment interaction produces spatial and temporal complexity of seismic behavior [*Huang and Turcotte*, 1990; *Ruff*, 1992]. More advanced, fully dynamic numerical rupture simulations including the effects of both coseismic and dynamic stress transfer based on rate and state friction revealed important insights for seismic hazard assessment [*Kaneko et al*., 2010; *Dublanchet et al*., 2013].

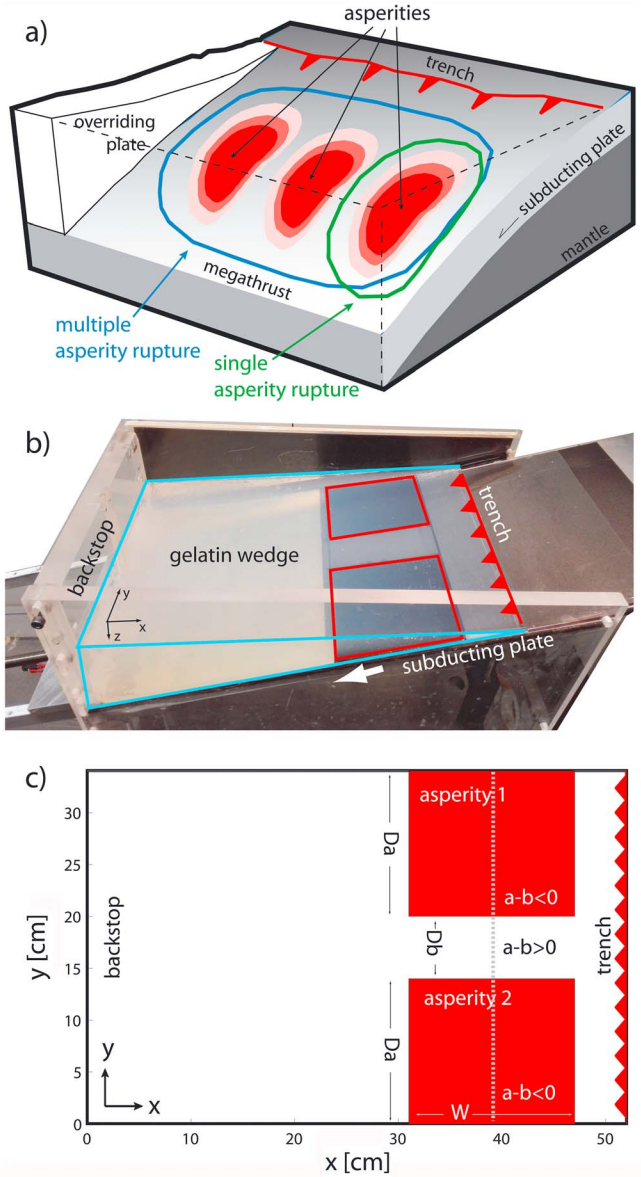

Figure 1. Sketch of a megathrust with asperities highlighted in red. (a) The green and blue contours indicate the rupture area of single- and multiple-asperities ruptures, respectively. (b) Photograph (oblique view) and (c) schematic representation (top view) of the experimental apparatus. The red rectangles represent the two asperities. The trench is highlighted by the red triangles. The gray dashed line represents the location of ruptures cross sections shown in Figure 2c.

These models have been used to investigate the probability that a seismic rupture overcomes barriers producing, in turn, a large magnitude earthquake. However, fully dynamic simulations in 3-D are computationally demanding, and, for this reason, the majority of the models are usually performed in 2-D.

Inspired by the numerical simulations of *Kaneko et al.* [2010], here we use complementary 3-D analog models specifically designed to investigate the control of asperities size and spacing on seismic behavior of a generic subduction megathrust. Our models feature scaled material properties (i.e., elasticity is scaled down to the natural prototype) and, with respect to most previous numerical models, more realistic 4-D boundary conditions (i.e., wedge-like geometry and presence of a free surface, gravity, time, and space continuum). A limitation, however, is imposed by the fact that analog earthquake ruptures are quasi-static (rupture velocity is ≈10% shear wave speed). Therefore, seismic waves are unlikely to be excited and dynamic effects not present. We adopted the "seismotectonic scale models" approach to develop our models, taking therefore into account geometric, kinematic, and dynamic similarity criteria [e.g., *Hubbert*, 1937; *Rosenau et al.*, 2017]. An important consequence of such scaling is the introduction of a dyadic time-scaling factor that allows slowing down the earthquake rupture process and speeding up the interseismic stress buildup phase, keeping dynamic similarity in both stages [*Rosenau et al.*, 2009; *Rosenau et al.*, 2017]. Despite the unavoidable experimental oversimplifications, the main advantages of analog models are: (a) the physically self-consistent behavior, which allows spontaneously nucleating analog earthquakes as a result of stress build-up and plates interface strength; (b) the capability of reproducing tens of seismic cycles in a convenient experimental time; and (c) the 3-D nature of the setup, which is mandatory for studying the synchronization process.

2. Experimental Setup and Monitoring

An elastic wedge made of pig skin gelatin analog of the overriding plate is underthrusted (with a velocity of 0.1 mm/s) by a planar, 10° dipping, rigid slab analog of the subducting plate (Figure 1b; see *Corbi et al.* [2013]

for additional details on the experimental apparatus and scaling). The model reproduces a convergent margin section 34 × 52 cm^2 (which is equivalent to 216 × 330 km^2 in nature) in trench-parallel and trench-orthogonal directions, respectively. The slab embeds two rectangular sandpaper patches creating stick-slip frictional behavior and acting as seismic asperities (Figures 1b and 1c; see *Corbi et al*. [2011] for details about frictional properties of gelatin on sandpaper). The downdip width $W = 16$ cm and the depth range (4.5–1 cm) of the asperities is kept constant according to the down scaled values of worldwide average of natural seismogenic zones [*Heuret et al*., 2011]. Analog asperities have identical geometrical, kinematic, and frictional properties (the friction rate parameter $a\text{-}b \approx -0.03$) and are separated by a velocity strengthening friction area ($a\text{-}b \approx 0.03$) acting as a barrier to slip propagation (Figure 2c). The along-strike length of the barrier (*Db*) and of the asperities (*Da*) are varied systematically in the 0–10 cm range and in the 6–17 cm range, respectively (Figure S1 in the supporting information). To ease the comparison with nature, we define the dimensionless asperities spacing parameter *Db/Da* which in our models ranges from 0 (i.e., models with no barrier) to 1.7. Experiments are monitored at 7.5 frames per second from top view for 22 min, allowing the observation of rupture behavior over several analog seismic cycles. Images are processed by means of particle image velocimetry PIV (MATPIV) [*Sveen*, 2004; *Adam et al*., 2005]. A MATLAB algorithm is used to compute analog earthquake source parameters from the PIV-derived velocity field (supporting information Text S1). To characterize the seismic behavior of our models we used the maximum earthquake magnitude (M_{max}), seismicity rate (τ), interseismic coupling (ISC), and percentage of earthquakes with synchronized failure of both asperities (*P*; see supporting Text S2 for the definition of M_{max}, τ, ISC, and *P*).

3. Experimental Observations and Interpretations

3.1. General Model Behavior

The model behavior is characterized by an initial 3–5 min long phase of slow, landward motion during which the gelatin wedge is loaded while shortening elastically by approximately 1–6% (0.5–3.0 cm). Once the maximum frictional strength of the stick-slip patches is reached, the system starts displaying seismic cycle behavior during which the models reproduce tens of trenchward slip episodes (analog to coseismic deformation) alternated by relatively longer and slower periods of landward displacement (analog to interseismic deformation stages; Figure 2a). Analog earthquake magnitudes range from M_w 6.5 to 8.4 (Figure 2b). The upper and lower magnitude limits are dictated by the size of the experimental setup and detection limit, respectively.

The models produce a suite of different events whose rupture: (a) nucleates and arrests within a single asperity (e.g., events 23 and 29; Figure 2c), (b) extends laterally for the whole asperity length and arrests at the barrier (e.g., events 24 and 28; Figure 2c), and (c) nucleates in one and involves both asperities, thus jumping the central barrier (event 31; Figure 2c).

Analyzing earthquakes behavior over subsequent seismic cycles, we recognize sequences of alternating failure of the two asperities (e.g., events 22–28 and 32–39; Figure 2c); clusters of repeating earthquakes where the same asperity ruptures more than once while the other remains quiescent (events 39–42); sequences of earthquakes that complement each other laterally thus unzipping progressively the analog megathrust (events 28–30); and synchronized failure of two asperities that may occur as a single event (event 31) or as a cluster of subsequent synchronized failures.

Figure 3 shows the details of two ruptures (source time functions are reported in Figure S2). Earthquake 31 nucleates at shallow depth and at ~1 cm from the model sidewall and rapidly (within 0.14 s) saturates the initial asperity. During the following ~0.8 s, the rupture propagates laterally with a velocity of about 20 cm/s activating the second asperity. During this stage, the majority of the slip still occurs on the initial asperity. At about 1.2 s the majority of slip shifts to the second asperity, while the asperity where the rupture initiated is progressively abandoned. The incremental slip history is characterized by two peaks occurring at 0.94 s and 1.47 s. This is due to a temporary rupture speed decrease associated to the involvement of the barrier and the subsequent acceleration occurring during the activation of the second asperity. The rupture process as a whole consists of two cracks (i.e., slip duration at a given point on the fault is 70–90% of the earthquake duration; Figure S3) offset in time. This results in a rupture that shifts laterally (i.e., in trench-parallel direction) from one asperity to another.

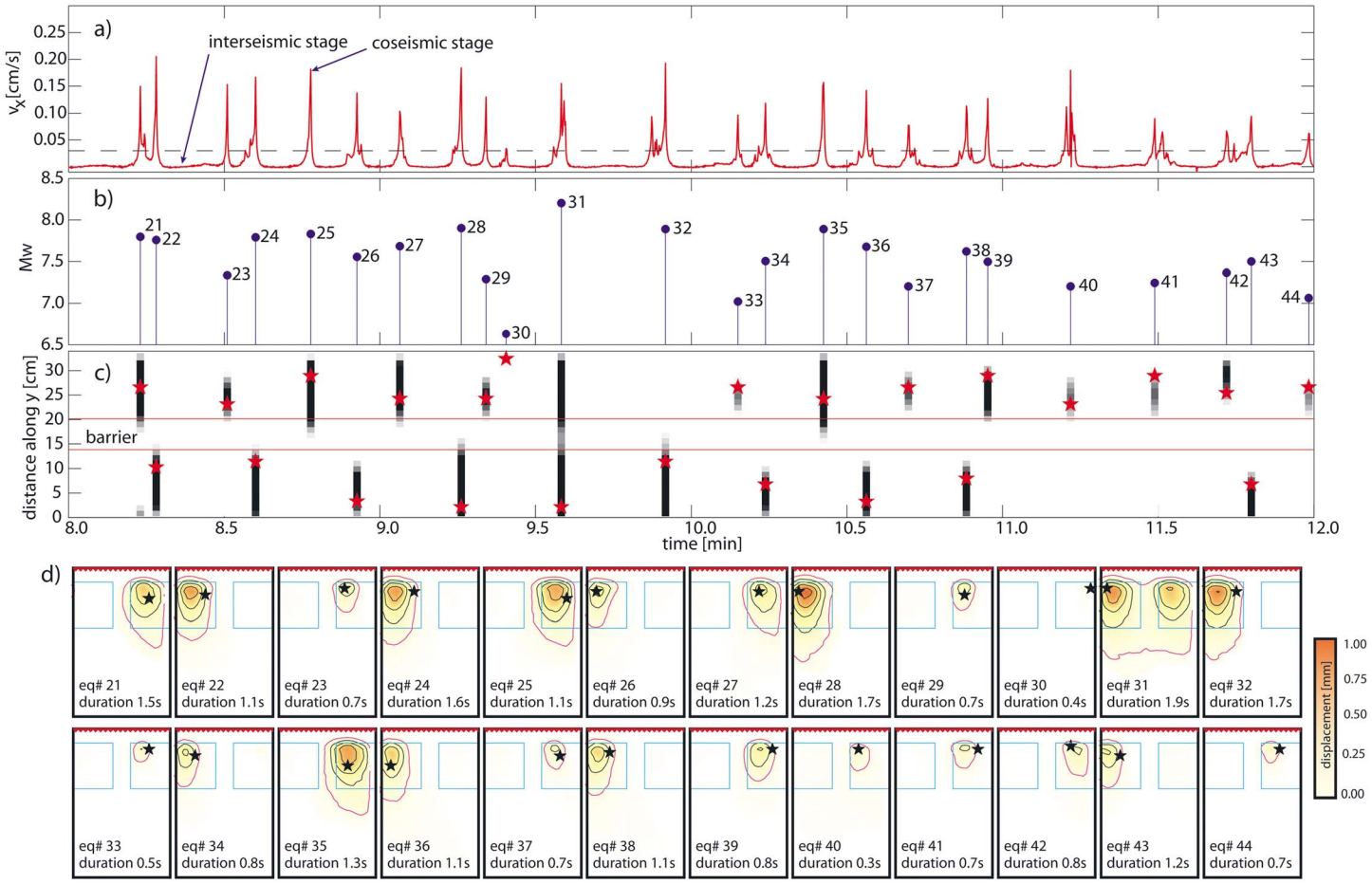

Figure 2. Model behavior shown by a 4 min long model run: time series of horizontal velocity (i.e., *x* component) measured at the model surface. (a) The dashed line represents the velocity threshold above which "coseismic" velocities are identified. Each velocity peak is associated to an earthquake magnitude M_w. (b) Numbering refers to earthquake number from the beginning of the experiment. Line-time seismic evolution of the model represented by a mid-depth cross section in *y* direction. Each thick vertical line represents the lateral extent of an earthquake. The red stars indicate the position of the hypocenters. (c) The two horizontal red lines highlight the position of the barrier. Surface displacement associated with individual earthquakes into shown in the previous panels. The magenta and black contour represent 0.15 mm and successive slip increments, respectively. (d) The black stars and the red triangles highlight the epicenter and the trench position, respectively.

Earthquake 32 also nucleates at shallow depth and close to the barrier but in this case the rupture remains confined in the initial asperity. The incremental slip history reveals a single peak of slip rate occurring at 1.34 s. The source time functions (Figure S2) reflect the asperity activation, showing a two-peak and single-peak signal for earthquake 31 and 32, respectively.

3.2. Control of *Db/Da* on Seismic Behavior

Fourteen models are realized with the specific goal of exploring the role of *Db/Da* on the selected seismic parameters. The resulting experimental earthquake catalogue includes 1237 analogue earthquakes which are used for the following parametric analysis.

Accordingly, M_{max} decreases linearly as a function of *Db/Da* ($R = 0.65$; Figure 4a), which is consistent with the link between earthquake magnitude and the asperities' size.

Similarly to M_{max}, τ shows a negative linear dependency to *Db/Da* ($R = 0.68$; Figure 4b). In general, models with relatively smaller asperities (large *Db/Da*) are associated with low values of interseismic coupling, or equivalently larger amount of creeping. Large creeping contribution increases the duration of the stress buildup phases to reach the fault frictional strength of the asperities, which results in smaller values of τ.

When $Db/Da < 0.5$, *P* decreases linearly as a function of *Db/Da* ($R = 0.65$; Figure 4d), highlighting that asperities synchronization is favored by closer and larger asperities. For $Db/Da < 0.1$, 50%–100% of the ruptures show asperities synchronization, which is consistent with a model without any barrier. When $Db/Da > 0.5$

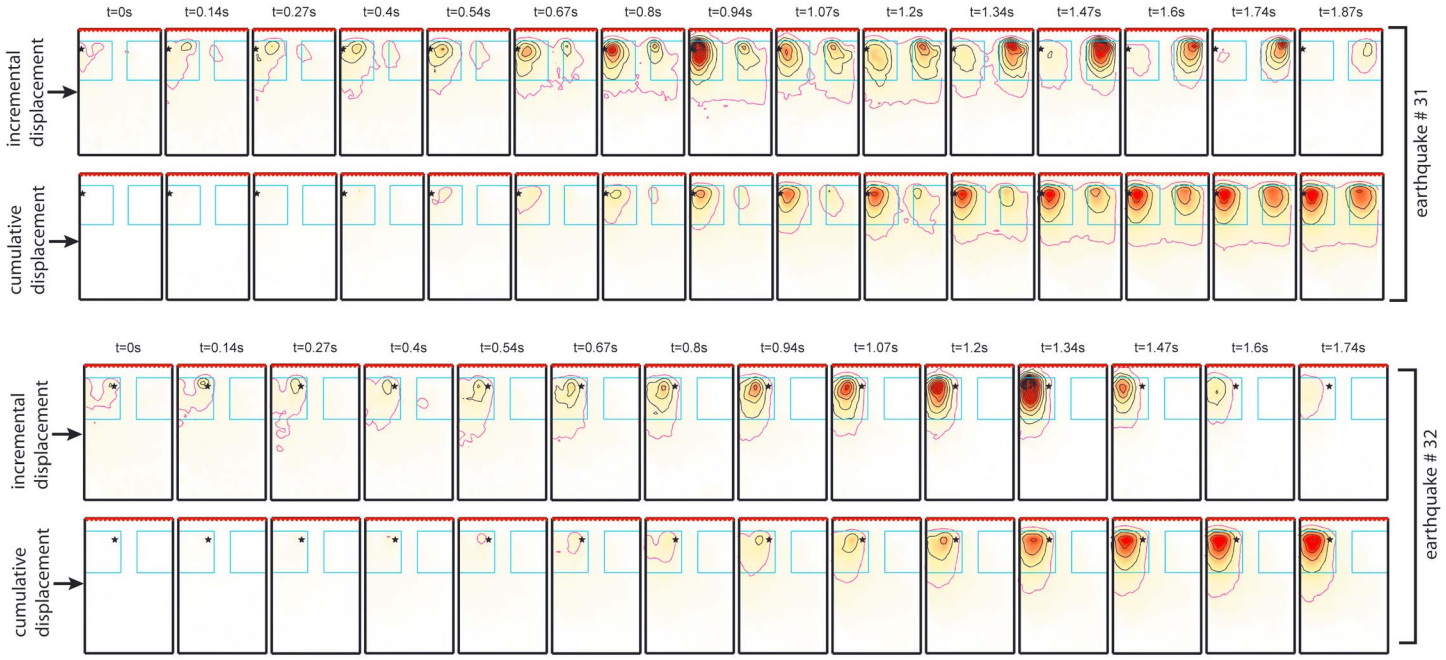

Figure 3. Incremental and cumulative maps of surface displacement associated with a synchronized asperities rupture (earthquake 31) and single asperity rupture (earthquake 32). Time from the beginning of the event is shown above each panel. Symbols, background shading, and contours as in Figure 2. The color scale and contour for incremental displacement is one tenth of the cumulative one.

none of the ruptures overcomes the velocity strengthening area, indicating the presence of a permanent barrier above this threshold.

4. Discussion

4.1. Plates Unzipping Mechanism

The process of asperities synchronization imaged in our experiments consists of two cracks offset in time while the earthquake grows laterally (Figure 3; earthquake number 31). Such rupture behavior shares profound similarities with the M_w7.8 Pedernales earthquake that hit the Ecuadorian megathrust in 2016. As in our models, the Pedernales earthquake features the rupture of two adjacent asperities that activated in two distinct phases of the same earthquake (i.e., the second asperity has been activated 25 s from earthquake initiation) [*Nocquet et al.*, 2016]. Also the M_w8.0 Pisco earthquake, which occurred in 2007 along the Peruvian megathrust, is characterized by rupturing of two distinct asperities with slip activation on the second asperity delayed by 60 s from earthquake initiation [*Sladen et al.*, 2010]. Another typical example of recent megathrust earthquake characterized by two slip patches is the M_w8.8 Maule earthquake that struck the central Chile megathrust in 2010 [*Moreno et al.*, 2012; *Lorito et al.*, 2011]. In this case, however, the rupture nucleated between two high slip patches and then propagated bilaterally. The amount of slip at the hypocentral area remained unchanged for more than the second half of earthquake duration [*Delouis et al.*, 2010] indicating that the majority of slip was occurring at the lateral edges of the rupture. Also, the 2007 Sumatra earthquake sequence shares similarities with our model of asperities synchronization. This sequence involved two events (M_w8.4 and M_w7.9) 12 h apart from each other, each consisting of two subevents. In particular, the M_w8.4 main shock shows unilateral rupture propagation and alternating activities of two slip patches (the southern one slipped during the first 40 s and the northern one slipped during the second 40 s) [*Konca et al.*, 2008]. The 2011 M_w9.0 Tohoku earthquake, with its peculiar behavior [*Avouac*, 2011; *Wang*, 2013], shows only partial overlap with the previous scenario. Although it has been proposed that it consisted of failure of three asperities [*Lee et al.*, 2011], its slip map shows only one large slip patch located in proximity of the hypocenter [e.g., *Ozawa et al.*, 2011; *Romano et al.*, 2014].

To recap, the activation of multiple asperities and the lateral (in trench-parallel direction) propagation as key ingredients for the triggering of great subduction megathrust earthquakes are therefore observed both in our models and in recent natural earthquakes.

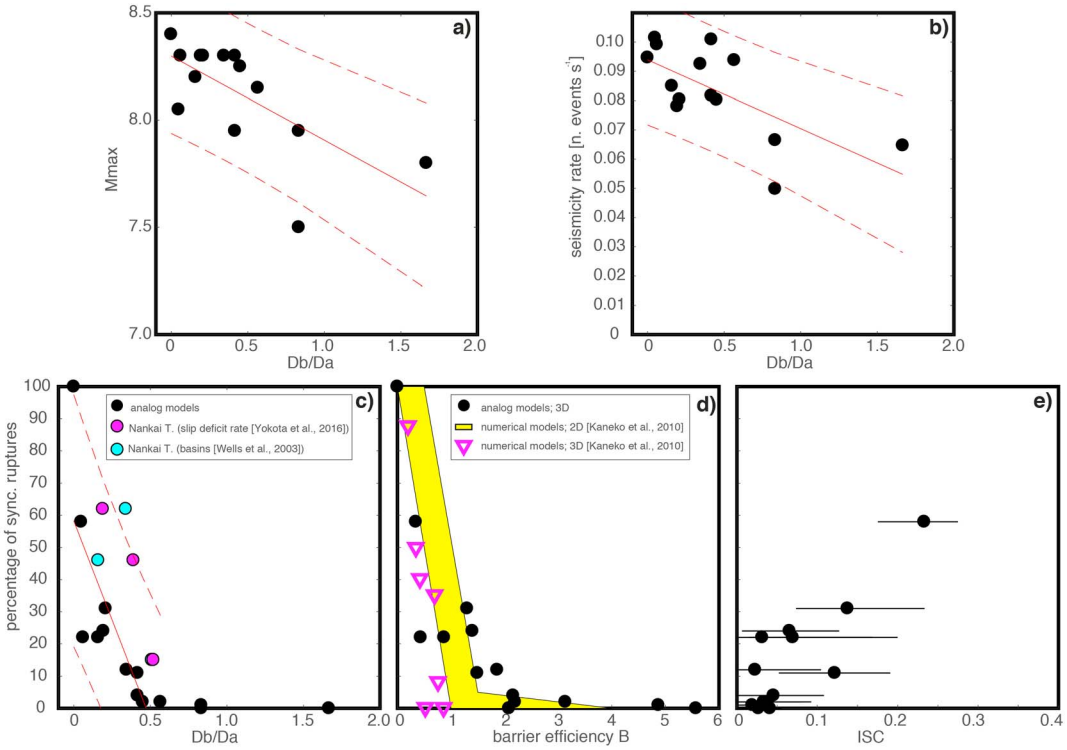

Figure 4. Control of *Db/Da* on seismic behavior. Plot of *Db/Da* versus (a) M_{max}, (b) seismicity rate, and (c) percentage of synchronized asperities ruptures. The solid and dashed red lines of Figures 4a–4c represent fit and 90% confidence interval, respectively. The percentage of synchronized asperities ruptures versus (d) barrier efficiency *B* and (e) interseismic coupling ISC (mean and first and third quartile shown by points and black lines).

4.2. Asperities Interaction and Synchronization

Our models highlight that the asperities spacing is one of the relevant parameters controlling megathrusts seismicity. In our models, low values of *Db/Da* are associated with larger M_{max} and higher τ. *Db/Da* has also a primary influence on the asperities synchronization process. Only when $Db/Da < 0.5$ the process of asperities synchronization has been observed and the number of synchronized events is inversely proportional to *Db/Da*. When $Db/Da > 0.5$, no synchronization is observed (Figure 4c). This dimensionless threshold must be considered valid under the experimental conditions as it may vary depending on *a-b* and normal stress as discussed afterward.

Aiming to quantify how asperities interact by means of stress coupling (or static stress transfer) in relation to the distance between them, we performed Coulomb stress modeling (using the MATLAB package Coulomb 3.3 [*Toda et al.*, 2005, *Lin and Stein*, 2004]). We calculated Coulomb stress changes for (trigger and receiver) patch geometries similar to those of our experiments, varying *Db/Da* in the 0.25–2 range (Figure S3). We find that the Coulomb stress change imposed by slip on a trigger patch in its near-field decays rapidly by more than 2 orders of magnitude within a distance of $Db/Da < 1$. Accordingly, Coulomb stress change on a receiver patch is about 1 ppm of the stress drop on the trigger patch for our experimentally identified threshold of $Db/Da = 0.5$. This suggests that asperities triggering by means of static stress change is effective under this configuration only for closely packed (i.e., $Db/Da < 0.5$) asperities. This calculation, however, neglects the stress due to previous seismic cycles providing therefore only a first-order constraint on the probability of synchronized asperities rupture occurrence.

Regarding the *Db/Da* control on asperities synchronization, our analog models confirm the outcomes of two recent studies based on numerical simulations of earthquakes on frictionally segmented faults [*Kaneko et al.*, 2010; *Dublanchet et al.*, 2013]. *Dublanchet et al.* [2013] used a model configuration made of several circular asperities embedded in a planar fault and identify a critical "asperities density" (defined as the amount of velocity weakening area with respect to the total fault area) needed to trigger a full fault rupture. Their study indicates that packed asperities favor the synchronization process. The concept of asperities density is useful

to constrain the process of seismic source interaction. However, it may be difficult to apply it to megathrust earthquakes, as small asperities are not properly resolved by geodetic monitoring methods, yet.

Kaneko et al. [2010] used numerical models having the same geometrical configuration as our study (i.e., planar fault with two asperities of equal size and friction) but additionally with variable strength of the barrier. Model behavior is described in terms of a dimensionless parameter *B*, which is the ratio of the stress increase required to the barrier for sustaining seismic slip to the coseismic stress drop (supporting information Text S2). *Kaneko et al*. [2010] show that for a given value of *Db*, a completely different seismic behavior can be achieved tuning normal stress and *a-b*. In particular, they show no asperities synchronization for moderately to little effective barriers when the spacing between asperities is larger than 25–50 km. This distance corresponds to $Db/Da \approx 0.35–0.70$ in our definition, corroborating the $Db/Da = 0.5$ found in our models. A quantitative comparison between analog and numerical models reveal the same inverse relationship between the percentage of synchronized ruptures and *B* (Figure 4d). This suggests that our analog models, even if performed under constant normal stress and *a-b* conditions, reproduce the full spectrum of seismic behavior observed in the numerical simulations.

Compared to asperities density, where knowledge of asperities distribution is needed, and *B*, where also frictional properties have to be known, *Db/Da* has the advantage of a straightforward applicability to nature. *Db/Da* may hide some degree of uncertainty for constraining the percentage of ruptures passing through the barrier as this depends also on normal stress and *a-b*; therefore, it must be used as a first-order proxy. Additional constrains for asperities synchronization may come from ISC. We report the average of ISC measured on the barrier area over subsequent seismic cycles as a function of the percentage of synchronized ruptures (Figure 4e). Despite the low absolute value of ISC (i.e., $ISC < 0.3$), models with higher percentages of synchronized rupture are characterized by relatively higher ISC. This behavior, which is in agreement with previous numerical models of *Kaneko et al*. [2010], suggests that the relative proportion of asperities versus barriers together with interseismic coupling may help in explaining earthquake diversity observed at subduction megathrusts.

4.3. Nankai Benchmark

We use the Nankai Trough for testing the reliability of *Db/Da* as a first-order proxy for synchronized failure in real subduction zones. Nankai Trough has a seismic record that dates back to thousands of years and is characterized by the occurrence of 13 megathrust earthquakes along a 530 km long segment of the subduction interface [*Ando*, 1975]. The Nankai segment is divided into four subsegments corresponding to four fore-arc basins [e.g., *Wells et al*., 2003]. Historical earthquakes involved one to four of those subsegments.

As a working hypothesis, we use two sets of tentatively related information, long-term and short-term, for constraining *Db/Da*: (a) trench-parallel extension of basins and distance between them [*Wells et al*., 2003] and (b) trench-parallel extension of areas of high slip deficit rate (i.e., >5 cm/yr) computed from seafloor geodetic measurements [*Yokota et al*., 2016]. Basins are hypothetically a geologic indicator of asperities [*Mogi*, 1969; *Nishenko and McCann*, 1979; *Wells et al*., 2003; *Fuller et al*., 2006; *Rosenau and Oncken*, 2009; *Rosenau et al*., 2017; *Saillard et al*., 2017], while high slip deficit rate zones highlight coupled locked areas of the megathrust where stress builds up during the monitoring period (i.e., the last 6 years in the case of Nankai).

For each data set (i.e., basins and slip deficit rate), we considered three test areas characterized by two asperities separated by a barrier (as in our models). Since the two asperities of a given test area have different sizes, we computed *Db/Da* using the trench-parallel extent of the larger asperity. This implies that for a given test area we consider the smaller *Db/Da*, or equivalently the scenario with the higher probability for synchronization.

We found $Db/Da \leq 0.5$ for all the three subregions of the Nankai segment using both data sets (Figure 4d). According to our models, this suggests the general possibility to experience synchronized asperities ruptures. In fact, a significant fraction of historical earthquakes, (i.e., 41% averaged over the whole Nankai segment) involved at least two subsegments. More specifically, we observe that five/six of Nankai test areas fall within the 90% confidence interval of the experimental trend (Figure 4d).

Our analysis has to be considered semiquantitative because of the involvement of uncertainties linked to potential variations of interseismic coupling in time and space and/or bias in historical rupture maps. However, the apparent good agreement identified supports our working hypothesis.

5. Conclusions

We used analog models for investigating the role of the size and the spacing of asperities on subduction megathrust seismicity. The barrier-to-asperities length ratio *Db/*Da displays a negative correlation with M_{max} and τ. *Db/Da* controls also the process of asperities synchronization. When *Db/Da* is <0.5, asperities synchronization has been observed in the models and the percentage of events with synchronized asperities rupture is inversely proportional to *Db/Da*. A permanent barrier, or equivalently no synchronization, is observed for *Db/Da* > 0.5. Our models suggest that the process of asperities synchronization occurs as a sequence of cracks activating at different times, allowing the rupture to grow laterally. We compared our model results with Nankai Trough historical seismicity for testing the reliability of *Db/Da* in controlling the asperities synchronization process. *Db/Da* is a relatively easily accessible parameter in nature given our increasing knowledge of the distribution of asperities and barriers from either short-term (coseismic slip and interseismic locking) or long-term (fore arc basins, ridges, and peninsulas) observations. Therefore, *Db/Da* should be taken into account for future studies focusing on parameters controlling the seismic behavior of subduction megathrusts.

Acknowledgments

This project has received funding from the European Union's Horizon 2020 research and innovation program under the Marie Sklodowska-Curie grant agreement 658034 (AspSync). M.R. has been supported by Deutsche Forschungsgemeinschaft (DFG) through grant CRC 1114 "Scaling Cascades in Complex Systems", Project B01. We thank reviewers J.P. Avouac and R. Jolivet for very constructive comments. We also acknowledge E. Rivalta, L. Passarelli, and L. Sandri for fruitful discussions, and R. Cattin also for providing the algorithm for inversion of surface deformation to fault slip. Data are available by contacting the corresponding author.

References

Adam, J., et al. (2005), Shear localisation and strain distribution during tectonic faulting—New insights from granular-flow experiments and high-resolution optical image correlation techniques, *J. Struct. Geol.*, *27*, 283–301, doi:10.1016/j.jsg.2004.08.008.

Ando, M. (1975), Source mechanisms and tectonic significance of historical earthquakes along the Nankai trough, Japan, *Tectonophysics*, *27*, 119–140, doi:10.1016/0040-1951(75)90102-X.

Avouac, J.-P. (2015), From geodetic imaging of seismic and aseismic fault slip to dynamic modeling of the seismic cycle, *Annu. Rev. Earth Planet. Sci.*, *43*(1), 150223150959000, doi:10.1146/annurev-earth-060614-105302.

Avouac, J. (2011), Earthquakes: The lesson of Tohoku-oki, *Nature*, *475*(16), 300–301, doi:10.1029/2009GL039276.

Chlieh, M., J. P. Avouac, K. Sieh, D. H. Natawidjaja, and J. Galetzka (2008), Heterogeneous coupling of the Sumatran megathrust constrained by geodetic and paleogeodetic measurements, *J. Geophys. Res.*, *113*, L21603, doi:10.1029/2007JB004981.

Corbi, F., F. Funiciello, C. Faccenna, G. Ranalli, and A. Heuret (2011), Seismic variability of subduction thrust faults: Insights from laboratory models, *J. Geophys. Res.*, *116*, B06304, doi:10.1029/2010JB007993.

Corbi, F., F. Funiciello, M. Moroni, Y. Van Dinther, P. M. Mai, L. A. Dalguer, and C. Faccenna (2013), The seismic cycle at subduction thrusts: 1. Insights from laboratory models, *J. Geophys. Res. Solid Earth*, *118*, 1483–1501, doi:10.1029/2012JB009481.

Delouis, B., J.-M. Nocquet, and M. Vallée (2010), Slip distribution of the February 27, 2010 M_w = 8.8 Maule Earthquake, central Chile, from static and high-rate GPS, InSAR, and broadband teleseismic data, *Geophys. Res. Lett.*, *37*, L17305, doi:10.1029/2010GL043899.

Dublanchet, P., P. Bernard, and P. Favreau (2013), Interactions and triggering in a 3-D rate-and-state asperity model, *J. Geophys. Res. Solid Earth*, *118*, 2225–2245, doi:10.1002/jgrb.50187.

Fuller, C. W., S. D. Willet, and M. T. Brandon (2006), Formation of forearc basins and their influence on subduction zone earthquakes, *Geology*, *34*(2), 65–68.

Heuret, A., S. Lallemand, F. Funiciello, C. Piromallo, and C. Faccenna (2011), Physical characteristics of subduction interface type seismogenic zones revisited, *Geochem. Geophys. Geosyst.*, *12*(1), 1–26, doi:10.1029/2010GC003230.

Huang, J., and D. Turcotte (1990), Evidence for chaotic fault interactions in the seismicity of the San Andreas Fault and Nankai trough, *Nature*, *348*, 234–236.

Hubbert, M. K. (1937), Theory of scale models as applied to the study of geologic structures, *Bull. Geol. Soc. Am.*, *48*(10), 1459–1520, doi:10.1130/GSAB-48-1459.

Kaneko, Y., J.-P. Avouac, and N. Lapusta (2010), Towards inferring earthquake patterns from geodetic observations of interseismic coupling, *Nat. Geosci.*, *3*(5), 363–369, doi:10.1038/ngeo843.

Konca, O., et al. (2008), Partial rupture of a locked patch of the Sumatra megathrust during the 2007 earthquake sequence, *Nature*, *456*(7222), 631–5, doi:10.1038/nature07572.

Lay, T., and H. Kanamori (1981), An asperity model of large earthquake sequences, *Earthq. Predict.*, *4*, 579–592.

Lay, T., H. Kanamori, and L. J. Ruff (1982), The asperity model and the nature of large subduction zone earthquakes, *Earthquake Predict. Res.*, *1982*(1), 3–71.

Lee, S.-J., B.-S. Huang, M. Ando, H.-C. Chiu, and J.-H. Wang (2011), Evidence of large scale repeating slip during the 2011 Tohoku-Oki earthquake, *Geophys. Res. Lett.*, *38*, L19306, doi:10.1029/2011GL049580.

Lin, J., and R. Stein (2004), Stress triggering in thrust and subduction earthquakes, and stress interaction between the southern San Andreas and nearby thrust and strike-slip faults, *J. Geophys. Res.*, *109*, B02303, doi:10.1029/2003JB002607.

Lorito, S., F. Romano, S. Atzori, X. Tong, A. Avallone, J. McCloskey, M. Cocco, E. Boschi, and A. Piatanesi (2011), Limited overlap between the seismic gap and coseismic slip of the great 2010 Chile earthquake, *Nat. Geosci.*, *4*(3), 173–177, doi:10.1038/ngeo1073.

Mogi, B. K. (1969), Relationship between the occurrence of great earthquakes and tectonic structures, *Bull. Earthquake Res. Inst.*, *47*, 429–451.

Moreno, M. S., J. Bolte, J. Klotz, and D. Melnick (2009), Impact of megathrust geometry on inversion of coseismic slip from geodetic data: Application to the 1960 Chile earthquake, *Geophys. Res. Lett.*, *36*, L16310, doi:10.1029/2009GL039276.

Moreno, M., et al. (2012), Toward understanding tectonic control on the M_w 8.8 2010 Maule Chile earthquake, *Earth Planet. Sci. Lett.*, *321–322*, 152–165, doi:10.1016/j.epsl.2012.01.006.

Moreno, M., M. Rosenau, and O. Oncken (2010), 2010 Maule earthquake slip correlates with pre-seismic locking of Andean subduction zone, *Nature*, *467*(7312), 198–202, doi:10.1038/nature09349.

Nishenko, S., and W. McCann (1979), Large thrust earthquakes and tsunamis: Implications for the development of fore arc basins, *J. Geophys. Res.*, *84*(B2), 573–584, doi:10.1029/JB084iB02p00573.

Nocquet, J.-M., et al. (2016), Supercycle at the Ecuadorian subduction zone revealed after the 2016 Pedernales earthquake, *Nat. Geosci.*, *10*, doi:10.1038/ngeo2864.

Ozawa, S., T. Nishimura, H. Suito, T. Kobayashi, M. Tobita, and T. Imakiire (2011), Coseismic and postseismic slip of the 2011 magnitude-9 Tohoku-Oki earthquake, *Nature*, *475*(7356), 373–376, doi:10.1038/nature10227.

Romano, F., E. Trasatti, S. Lorito, C. Piromallo, A. Piatanesi, Y. Ito, D. Zhao, K. Hirata, P. Lanucara, and M. Cocco (2014), Structural control on the Tohoku earthquake rupture process investigated by 3D FEM, tsunami and geodetic data, *Sci Rep*, *4*, 5631, doi:10.1038/srep05631.

Rosenau, M., and O. Oncken (2009), Fore-arc deformation controls frequency-size distribution of megathrust earthquakes in subduction zones, *J. Geophys. Res.*, *114*, B10311, doi:10.1029/2009JB006359.

Rosenau, M., F. Corbi, and S. Dominguez (2017), Analogue earthquakes and seismic cycles: Experimental modelling across timescales, *Solid Earth*, *8*(1), 1–12, doi:10.5194/se-8-1-2017.

Rosenau, M., J. Lohrmann, and O. Oncken (2009), Shocks in a box: An analogue model of subduction earthquake cycles with application to seismotectonic forearc evolution, *J. Geophys. Res.*, *114*, B01409, doi:10.1029/2008JB005665.

Ruff, L. J. (1992), Asperity distributions and large earthquake occurrence in subduction zones, *Tectonophysics*, *211*(1–4), 61–83, doi:10.1016/0040-1951(92)90051-7.

Ruff, L. J. (1996), Large Earthquakes in Subduction Zones: Segment Interaction and Recurrence Times, in *Subduction Top to Bottom*, edited by G. E. Bebout et al., AGU, Washington, D. C., doi:10.1029/GM096p0091.

Saillard, M., L. Audin, B. Rousset, J. P. Avouac, M. Chlieh, S. R. Hall, L. Husson, and D. L. Farber (2017), From the seismic cycle to long-term deformation: Linking seismic coupling and Quaternary coastal geomorphology along the Andean megathrust, *Tectonics*, *36*, 241–256, doi:10.1002/2016TC004156.

Scholz, C. H. (1998), Earthquakes and friction laws, *Nature*, *391*(6662), 37–42, doi:10.1038/34097.

Scholz, C. H., and J. Campos (2012), The seismic coupling of subduction zones revisited, *J. Geophys. Res.*, *117*, B05310, doi:10.1029/2011JB009003.

Schurr, B., et al. (2014), Gradual unlocking of plate boundary controlled initiation of the 2014 Iquique earthquake, *Nature*, doi:10.1038/nature13681.

Sladen, A., H. Tavera, M. Simons, J. P. Avouac, A. O. Konca, H. Perfettini, L. Audin, E. J. Fielding, F. Ortega, and R. Cavagnoud (2010), Source model of the 2007 M_w 8.0 Pisco, Peru earthquake: Implications for seismogenic behavior of subduction megathrusts, *J. Geophys. Res.*, *115*, B02405, doi:10.1029/2009JB006429.

Subarya, C., M. Chlieh, L. Prawirodirdjo, J.-P. Avouac, Y. Bock, K. Sieh, A. J. Meltzner, D. H. Natawidjaja, and R. McCaffrey (2006), Plate-boundary deformation associated with the great Sumatra-Andaman earthquake, *Nature*, *440*(7080), 46–51, doi:10.1038/nature04522.

Sveen, J. K. (2004), An introduction to MatPIV v.1.6.1 Eprint no. 2, ISSN 0809-4403, Dep. of Mathematics, University of Oslo. [Available at http://www.math.uio.no/~jks/matpiv.]

Tilmann, F., et al. (2016), The 2015 Illapel earthquake, central Chile: A type case for a characteristic earthquake? *Geophys. Res. Lett.*, *43*, 574–583, doi:10.1002/2015GL066963.

Toda, S., R. S. Stein, K. Richards-Dinger, and S. Bozkurt (2005), Forecasting the evolution of seismicity in southern California: Animations built on earthquake stress transfer, *J. Geophys. Res.*, *110*, B05S16, doi:10.1029/2004JB003415.

Wang, K. (2013), Megathrust surprises, *Nat. Geosci.*, *6*(1), 11–12, doi:10.1038/ngeo1682.

Wang, K., and S. L. Bilek (2014), Invited review paper: Fault creep caused by subduction of rough seafloor relief, *Tectonophysics*, *610*, 1–24.

Wells, R. E., J. Blakely, Y. Sugiyiama, D. Scholl, and P. Dinterman (2003), Basin-centered asperities in great subduction zone earthquakes: A link between slip, subsidence, and subduction erosion?, *J. Geophys. Res.*, *108*(B12), 167–171, doi:10.1029/2003JB002880.

Yokota, Y., T. Ishikawa, S. Watanabe, T. Tashiro, and A. Asada (2016), Seafloor geodetic constraints on interplate coupling of the Nankai Trough megathrust zone, *Nature*, *534*(7607), 374–377, doi:10.1038/nature17632.